Chapter 6
Predicting the Fundamental Period of Light-Frame Wooden Buildings by Employing Bat Algorithm-Based Artificial Neural Network

Mehdi Nikoo
Department of Building, Civil and Environmental Engineering, Concordia University, Montréal, Canada

Ghazanfarah Hafeez
https://orcid.org/0000-0002-5045-6968
Department of Building, Civil and Environmental Engineering, Concordia University, Montréal, Canada

Ghasan Doudak
Department of Civil Engineering, University of Ottawa, Ottawa, Canada

Vagelis Plevris
https://orcid.org/0000-0002-7377-781X
Department of Civil and Architectural Engineering, Qatar University, Doha, Qatar

ABSTRACT

The study utilizes an artificial neural network model for determining the fundamental period of Light-Frame Wooden Buildings, employing the Bat algorithm on a data set of 71 measured periods of wooden buildings. The number of stories, floor area, storey height, maximum length, and maximum width are selected as input parameters to estimate the fundamental period of light-frame wooden buildings. The accuracy and the competitiveness of the developed model were evaluated by comparing it with a similar particle swarm optimization (PSO)- ANN scheme, the formulas provided in the National Building Code of Canada, an equation obtained from the Eureqa software, and a non-linear regression (NLR) model. The results of the research show that the bat-ANN model exhibited the best overall performance with the lowest RMSE and MAE error values and the highest values of the Coefficient of determination, R^2, in comparison to the other examined models. Therefore, the proposed Bat-ANN model can be considered as a reliable, robust, and accurate tool for predicting the fundamental period of wooden buildings.

DOI: 10.4018/978-1-6684-5643-9.ch006

INTRODUCTION AND BACKGROUND

Reliable seismic analysis and design of a structure require precise knowledge about the fundamental period of the building, among other dynamic characteristics. Building codes around the world provide simplified formulas for estimating the fundamental periods of buildings constructed with different materials, structural systems and geometries (Panthi et al., 2021). The National Building Code of Canada (NBCC) provides empirical formulas to calculate the fundamental lateral period of vibration of different structural systems, such as shear walls, steel moment-resisting frames, reinforced concrete moment resisting frames, and steel braced frames (NRC/IRC, 2015). The formula for shear walls can also be applied to what is termed in the code as “other structures” and it is only a function of building height above the base, h_n, as presented in Eq. (1).

$$T_a = 0.05h_n^{3/4} \tag{1}$$

Proper estimates of the fundamental period is imperative in seismic analysis and design as it is the basis for the calculation of the design base shear and any error in estimating the fundamental period could have significant consequences in over- or under- estimating the seismic forces, leading to an overly conservative or unsafe design. An alternative method for calculating the building period, which is permitted by the NBCC is using numerical methods, such as Rayleigh’s method or eigenvalue analysis. The drawback of using such methods is their association with uncertainty in input parameters, especially pertaining to the stiffness of the structural system, as well as some limitations related to lower bound limits imposed on the base shear.

It has been well recognized that considering the building height as the only variable describing the dynamic characteristics of a building and to approximate the period based only on the height is not sufficient. Several investigations have been conducted to evaluate the adequacy of these equations on concrete, steel and wooden buildings, and several authors have suggested improved equations. The subsequent section provides the state-of-the-art knowledge on building periods established based on field measurements and using finite element analysis methods. In the present study, an ANN model employing the Bat Algorithm is developed to provide a better prediction of the fundamental period of light-frame wooden buildings including several additional parameters to the building height. While similar approaches can be found in the literature, the methodologies used in these studies are limited to mainly concrete structures (Plevris & Solorzano, 2021; Solorzano & Plevris, 2021). In the current study, the model exhibiting the best performance is selected from a set of examined ANN models and subsequently compared with other models, such as ANN-Particle Swarm Optimization, Nonlinear regression, the NBCC (NRC/IRC, 2015), as well as equations derived from the Eureqa software (Dubčáková, 2011; Schmidt & Lipson, 2009).

LITERATURE REVIEW

The majority of the available literature on experimental studies with aim to investigate the fundamental period of existing buildings have been focused on concrete structures, while limited studies are available for steel and wooden buildings. The proposed equations have primarily depended on the seismic force resisting system (SFRS) typology, material types which relates to the building mass, and overall building geometry. Farsi and Bard (Farsi & Bard, 2004), Lagomarsino (Lagomarsino, 1993) and Gilles (Gilles, 2011) performed ambient vibration tests (AVT) on several reinforced concrete shear wall buildings and suggested improved relationships for estimating the building periods required for the calculation of the base shear in seismic design. The proposed equations were limited to linear expressions with the height of the buildings. The period equations suggested by other authors for reinforced concrete shear wall buildings, such as Goel and Chopra (Goel Rakesh & Chopra Anil, 1997), Lee et al. (Lee et al., 2000), Morales (Dominguez Morales, 2000) provided expressions with multiple variables and were not limited to building height.

The study undertaken by Goel and Chopra (Goel Rakesh & Chopra Anil, 1997) assessed the code period equation for shearwall buildings specified in the US building codes (NEHRP 94, SEAOC 96 and UBC 1997) by investigating the fundamental periods measured during strong ground motions. The authors reported a significant scatter in the measured period and suggested an improved expression based on regression analyses of experimental results from nine shear wall buildings that included variables related to shear wall dimensions, such as height and equivalent shear area (Eq. (3) in Table 1). Similarly, Lee et al. (Lee et al., 2000) focused on evaluating the period formula in the Korean building code by employing fundamental period data-set of fifty reinforced concrete shear wall buildings. The periods were measured using ambient vibration testing, and the proposed relationship for estimating the period derived for a uniform cantilever shear beam is shown in Eq. (4).

Morales (Dominguez Morales, 2000) evaluated the code period equation for concrete shear walls and frame buildings and proposed an equation that accounted for the moment of inertia (equivalent second moment of area) and height of the building. The equation was linear regarding the height but nonlinear with the moment of inertia and demonstrated a reasonable correlation with the measured periods. The proposed equation (Eq. (6) in Table 1) was derived from the database of the buildings whose fundamental periods were measured during strong earthquake motions by the California Strong Motion Instrumentation Program (CSMIP) and by the National Oceanic and Atmospheric Administration (NOAA). It should be noted that the dataset used in this study was mostly similar to that employed by Goel and Chopra (Goel Rakesh & Chopra Anil, 1998) in establishing Eq. (3).

Gilles et al. (Gilles et al., 2011) created a database of 27 reinforced concrete buildings and proposed an improved relationship for the fundamental period of concrete shear wall buildings as a function of the building height. The improved equation was found to provide better estimates when compared to the equations provided in the code and other improved models available in the literature. Models to estimate the vibration period of torsion, second modes and models that could account for the uncertainty associated with fundamental period were also proposed in this study.

Efforts have also been made to investigate the applicability of code equations to wooden shear wall buildings. Camelo (Camelo et al., 2001) proposed a period formula based on a non-linear expression as a function of the building height. The proposed equation was capable of predicting the period of wooden buildings more accurately than the period formula provided in Uniform Building Code (UBC 97) (Paz & Leigh, 2004). Hafeez et al. (Hafeez et al., 2018, 2019; Hafeez et al., 2014) developed a comprehensive database of measured dynamic properties of light-frame wooden buildings based on ambient vibration tests. The study assessed the adequacy of the NBCC code formula for approximating the fundamental period of wooden shear wall buildings. The suggested equation was non-linear with building height, shear wall length and floor area.

Table 1 summarizes the experimental studies that provided alternative expressions to calculate the fundamental period of shear wall buildings for different materials. The studies reported in Table 1 emphasize the need to include more sophisticated approaches with several parameters in order to obtain a better estimate of the fundamental period. One of the issues associated with testing several buildings in order to develop an approximation of their behaviour is that the buildings are very complex systems that even when multiple parameters are included in the analysis, it does not guarantee the adequacy of the proposed model. Also, typically the effect of the individual parameters is not assessed separately. This has made assessment procedures like ANN a useful alternative as will be demonstrated in this study.

Table 1. Equations proposed for estimating the fundamental period of shear wall buildings

(Author, Year)	Material	Proposed Equation	Eq.	Parameters	Method
(Lagomarsino, 1993)	Concrete	$T_1=0.018H$	(2)	H: Height of the building	Ambient vibration
(Goel Rakesh & Chopra Anil, 1997)	Concrete	$T=\frac{0.0062h}{\sqrt{A_e}}$	(3)	A_e: Area of the floor h: Height of the building	Earthquake Records
(Lee et al., 2000)	Concrete	$T=0.4\left[\frac{h^{0.2}}{\sqrt{L_w}}\right]$	(4)	h: Height of building (m) L_w: Total wall width per unit plan area (m^{-1})	Ambient vibration
(Farsi & Bard, 2004)	Concrete	$T_1=0.01h$	(5)	h: Height of the building	Ambient vibration
(Dominguez Morales, 2000)	Concrete	$T=0.13\frac{h}{I^{0.25}}-0.4$	(6)	h: height of the building I: Moment of inertia	FEA and linear regression
(Gilles et al., 2011)	Concrete	$T=0.020h$	(7)	h: Height of the building	Ambient vibration
(Hafeez et al., 2018)	Wood	$T=0.045(\frac{h}{l}\mathrm{A})^{0.36}$	(8)	H: Building height A: Building area l: Shear wall length	Ambient vibration
(Camelo et al., 2001)	Wood	$T=0.032h_n^{0.55}$	(9)	h_n: Building height (ft)	Forced vibration

During the last years, there has been an increasing trend in employing ANN for the solution of complex problems in various scientific fields, including economics, engineering, and many others. In the field of structural engineering particularly, ANN has been successfully applied to solve various engineering problem (Lagaros & Papadrakakis, 2004; Plevris & Tsiatas, 2018). Examples of ANN having been successfully applied includes the modeling of masonry failure (P.G. Asteris & V. Plevris, 2013; Panagiotis G. Asteris & Vagelis Plevris, 2013; Asteris & Plevris, 2017; Plevris & Asteris, 2015; V. Plevris & P.G. Asteris, 2014; Vagelis Plevris & Panagiotis G. Asteris, 2014; Plevris et al., 2017; Plevris et al., 2019), predicting the compressive strength of concrete containing recycled aggregate (Dabiri et al., 2022; Kandiri et al., 2021), modeling the corrosion rate in cables of suspension bridges (Ben Seghier et al., 2021), predicting the properties of FRP-Confined Concrete Cylinders (Ahmad et al., 2020), determining the nominal shear capacity of steel fiber reinforced concrete beams (Ahmadi et al., 2020), predicting the bond stress of corroded steel reinforcing bars in concrete members (Ahmadi et al., 2021), and predicting the capacity of concrete walls (Sharib et al., 2021). ANN has also been successfully used for modeling and analyzing wooden structures, such as for predicting the compression strength of heat treated woods (Tiryaki & Aydın, 2014), predicting the mechanical properties of wood (Fathi et al., 2020) and investigating wood bonding quality based on pressing conditions (Bardak et al., 2016), among other interesting and innovative applications.

ARTIFICIAL INTELLIGENCE AND OPTIMIZATION ALGORITHMS

Artificial Neural Networks

An ANN consists of an input layer and an output layer and between them there exist a number of hidden layers that execute factual processing through weighted connections between the neurons of each layer. In a fully connected ANN model, each neuron of a layer is connected to every neuron of the next layer. The final, output layer is used to obtain the processing outcomes (Plevris, 2009).

A feed-forward neural network is an ANN in which nodes do not form a directed cycle. The information in this network flows solely in one direction from the input nodes to the output nodes, passing through the nodes of the hidden layers. The feed-forward network comprises several layers of computing units, coupled in a feed-forward manner. Each neuron in one layer is connected to neurons in the adjacent layer via directed connections. In many applications, these networks' units use the sigmoid, tangent sigmoid, purelin (Linear), poslin (Positive linear), and log sigmoid transfer functions as activation functions (Pham & Liu, 1995).

Bat Algorithm

The bat optimization technique was inspired by the tracking properties of little bats seeking prey and specifically the behavior of bats when they reflect sound. The Bat algorithm begins by establishing a population of bats and determining their global optimum position in the search space using a fitness cost function. Each bat's position is decided by a random step toward the global optimum position. If a bat receives a signal from the global best location during an iteration, it will migrate towards that location. In each iteration, if the calculated new position of each bat improves the value of the fitness function for that bat, then the new position is saved. The algorithm iterates until a stop criterion is reached (Dehghani & Bogdanovic, 2018). This approach is also suitable for training an ANN. The network's weights and biases are considered as the design variables of the optimization problem, i.e. the position vector of a bat, and so each bat population represents a phase of the ANN training. The network's prediction error is assigned as the bat's cost function value, which needs to be minimized. In this sense, the bat algorithm's final solution represents a fully trained network (Dehghani & Bogdanovic, 2018).

The Bat algorithm initially generates a random population of bats and then changes its frequency using Eq. (10) (Aalimahmoody et al., 2021; Dehghani & Bogdanovic, 2018):

$$f_i = f_{min} + (f_{max} - f_{min})\beta \tag{10}$$

where f_i denotes the frequency of the i-th bat, f_{min} denotes the minimum frequency, f_{max} denotes the maximum frequency, and β is a random value between 0 and 1. The bats' position and velocity are updated using Eqs (11) and (12) (Srivastava & Sahana, 2019):

$$V_i^{t+1} = V_i^t + \left(x_i^t - \mathrm{x}^*\right) f_i \tag{11}$$

$$x_i^{t+1} = x_i^t + V_i^{t+1} \tag{12}$$

where V_i^t is the velocity of the i-th bat at iteration t, x_i^t is the position of the i-th bat at iteration t, and x^* is the global best position of the entire bat population.

The technique then uses Eq. (18) to relocate some bats towards the best global location (Shadbahr et al., 2021).

$$x_{new} = x_{old} + \varepsilon \mathrm{A} t \tag{13}$$

where A represents the loudness and ε is a random value between 0 and 1.

The cost function value of each bat's new position must be smaller than the one of the previous iterations. Following that, the algorithm modifies the pulse rate and volume using Eqs (20) and (21) (Dehghani & Bogdanovic, 2018):

$$A_i^{t+1} = \alpha A_i^t \tag{14}$$

$$r_i^{t+1} = r_i^0 \left(1 - \exp\left(-\gamma t\right)\right) \tag{15}$$

where α is a constant between 0 and 1, r^0_i is the initial pulse rate, and γ is a constant value.

Particle Swarm Optimization

Particle swarm optimization (PSO) is a metaheuristic algorithm inspired by the behavior of swarms of animals (e.g., flock of birds) (Kennedy & Eberhart, 1995). Generally, random solutions are used to initialize the algorithm. The algorithm's potential solutions, referred to as particles, possess particular positions and velocity vectors in the design space. The particles have a "memory" as they are able to "remember" the best cost function value associated with the locations they have individually visited (local best solution). Additionally, the algorithm tracks the best solution produced thus far by the entire swarm, referring to it as the global best solution (Plevris & Papadrakakis, 2011). The particle swarm optimization algorithm changes the velocity and the position of particles throughout the iterations thus taking them closer to their local and global optimal solutions. A random weight term is used to account for the influence of local best and global best solutions. In the ANN-PSO approach, the PSO optimizer is used for training the ANN, i.e. finding the values of the network's weights and biases that lead to the minimization of the prediction error.

Performance Metrics

To determine the model's accuracy, statistical metrics (error metrics) need to be used. These metrics help identify the best models which exhibits the least error and has the most generalization capabilities. The root mean squared error (RMSE) and the mean absolute error (MAE) are the statistical metrics used in this study to assess the accuracy of the various models, as presented in Eqs. (16) and (17) (Li & Heap, 2008):

$$RMSE = \left[\frac{1}{n} \sum_{i=1}^{n} \left(C_i - O_i \right)^2 \right]^{\frac{1}{2}} \tag{16}$$

$$MAE = \frac{1}{n} \sum_{i=1}^{n} \left| C_i - O_i \right| \tag{17}$$

where C_i and O_i define the calculated (model predicted), and the observed (ground truth) data, respectively, and n is the number of samples in the database. In addition, we also take into account the Coefficient of determination (R^2), a number between 0 and 1 that measures how well a statistical model predicts an outcome (Plevris et al., 2022).

METHODOLOGY

Dataset

The measured period database used in this study is obtained from past studies on the estimation of the period of wooden buildings (Hafeez et al., 2018, 2019; Hafeez et al., 2014). The authors of these studies investigated the buildings' response under low amplitude motion, where the responses of several buildings with various geometric configurations were measured using ambient vibration method. The recorded motions of the buildings were analyzed in the frequency domain to extract the modal parameters including frequency, mode shape and damping ratio. This study employs 71 samples with various input parameters to establish an expression for the fundamental period of light-frame wood buildings. The input parameters include number of stories, total building height, plan area and the maximum length and width on the building plan (where the plan dimensions are irregular). The statistical properties related to the input parameters are shown in Table 2.

Figure 1 provides an overview of the structural period distribution in the range of 0.11 s to 0.45 s, which shows that approximately 79% of the period data is less than 0.3 seconds. Furthermore, Figure 2 shows a normal distribution curve demonstrating that the distribution of the fundamental period ranges mostly between 0.15 and 0.3 seconds.

Table 2. Statistical properties of the light-frame wooden building parameters

Statistical Index	Unit	Type	Min	Max
Stories	Number	Input	1	6
Total height	m	Input	3.00	21.60
Max length	m	Input	6.00	96.00
Max width	m	Input	4.90	80.00
Area	m^2	Input	29.89	7680.00
Period	s	Output	0.11	0.45

Figure 1. The experimental data's fundamental period distribution

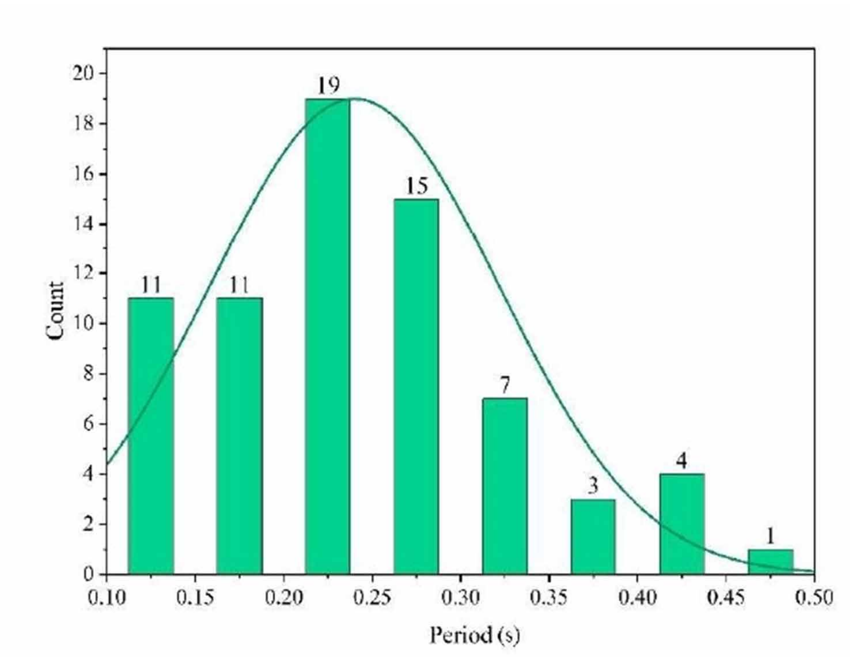

The correlation matrix of the input and output variables used in this study is presented in Figure 3, indicating a greater influence of the building height and the number of stories on the period of the building.

The subsequent section provides the details about various NN architectures developed employing optimization algorithms (Bat, PSO) used in this study, followed by the regression model (NLR), equations based on Eureqa software and the NBCC code model. Finally, the comparison among various best-performed models is discussed, and the conclusions of the study are presented.

Unlike a correlation plot, a Variation Inflation Factor (VIF), displayed in Eq. (18), is a measure to identify the multicollinearity of variables within the dataset. When correlation is considered among more than one variable, VIF will be the preferred method for estimating the variance of a regression coefficient. The value of VIF varies from 1, 1-5 and >10, indicating no, moderate and high correlation between the variables. Table 3 displays the evaluation of the correlation between variables with the VIF metric. As shown in the table, in most cases variables appear to be somehow correlated, having VIF values greater than 1, although in some cases the value is very close to 1 denoting practically no correlation.

$$VIF = \frac{1}{1 - R^2} \tag{18}$$

Figure 2. Box normal plot for the fundamental period

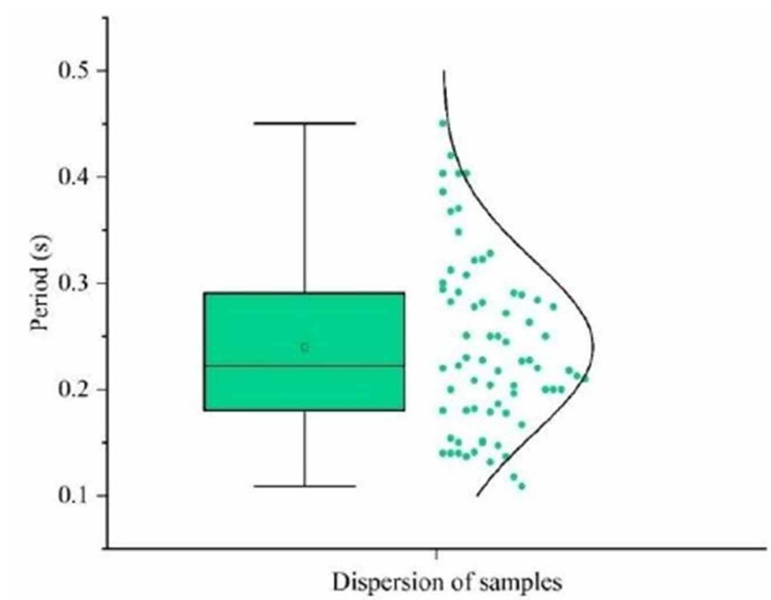

Figure 3. Correlation matrix for the input and output variables

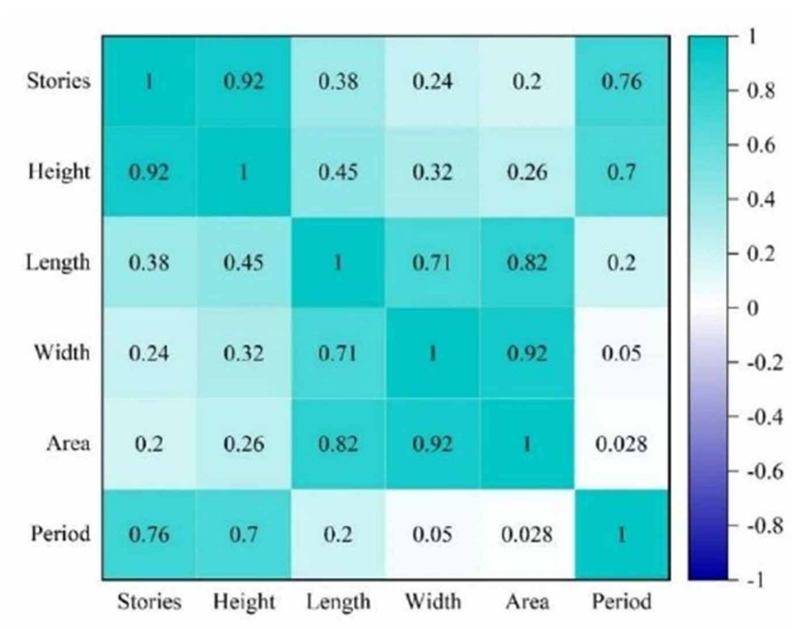

Table 3. Evaluation of correlation between variables with Variation Inflation Factor (VIF)

	Stories	Height	Max length	Max width	Area	Period
Stories						
Height	6.641					
Max length	1.171	1.258				
Max width	1.060	1.114	1.990			
Area	1.041	1.073	3.110	6.170		
Period	2.342	1.968	1.042	1.003	1.001	

ANN Model Combined With Bat Algorithm

A Feed-Forward type ANN is employed for calculating the fundamental period of the 71 samples of light-frame wooden buildings. The data were arbitrarily separated into two sets, as follows: 80% (57 samples) of the samples data were dedicated to the network training while the remaining 20% (14 samples) was reserved for network performance testing. In the development of the ANN model, the number of hidden layers and the number of neurons were selected based on the complexity of the problem, and Eq. (19) was used to obtain an estimate of the total number of neural cells of an ANN (Bowden et al., 2005).

$$N_H \leq \min(2N_I + 1) \tag{19}$$

where N_H denotes the number of nodes of the hidden layer, and N_I denotes the number of inputs. Given the five inputs, according to Eq. (19) the minimum number of nodes at each hidden layer should be 11. A number of different ANN architectures with two hidden layers are examined, as presented in Table 4. The first hidden layer has two to six neurons, and the second hidden layer has two to five neurons. For all ANNs, different transfer functions, including sigmoid, tangent sigmoid, purelin (Linear), poslin (Positive linear), and log sigmoid, have been used for the hidden and the output layers, as shown in the table. The Bat Algorithm was employed to adjust the weights and biases in order to minimize the prediction error, along with ANN training. Table 4 describes the different ANN topologies (16 in total) used in the study, while Table 5 describes the properties of the Bat Algorithm. The optimization parameters employed for reducing the errors in the ANNs weights of the Bat algorithm, shown in Table 5, were chosen based on recommendations from a previous study (Aalimahmoody et al., 2021).

All 16 ANN models were optimized using the Bat algorithm and their performances were assessed using three statistical indices, namely *MAE*, *RMSE* and R^2. Table 6 provides the top three models and the corresponding statistical assessment measures, as well as the slope of the straight line, used for the training and the testing sets.

In Table 6, the inclusion of "2L" in the topology refers to the presence of two hidden layers and the numbers in parentheses indicate the number of neurons in each hidden layer. It can be observed that the Bat-ANN 2L (4-3) network has the lowest *MAE* and *RMSE* index in the training and testing phases. It also has the highest R^2 value in both the training and testing phase (0.96 and 0.95, respectively) which indicates that the model is the most accurate among the 16 models of this study. The corresponding Bat-ANN 2L (4-3) network topology is shown in Figure 4.

Table 4. Different topologies used in ANN training

No	Topology	Hidden and Output Activations	No	Topology	Hidden and Output Activations
1	5-6-5-1	TANSIG-PURELIN	9	5-4-5-1	LOGSIG-PURELIN
2	5-6-4-1	PURELIN-PURELIN	10	5-4-4-1	TANSIG-TANSIG
3	5-6-3-1	POSLIN-PURELIN	11	5-4-3-1	TANSIG-PURELIN
4	5-6-2-1	LOGSIG-PURELIN	12	5-4-2-1	PURELIN-PURELIN
5	5-5-5-1	TANSIG-TANSIG	13	5-3-5-1	POSLIN-PURELIN
6	5-5-4-1	TANSIG-PURELIN	14	5-3-4-1	LOGSIG-PURELIN
7	5-5-3-1	PURELIN-PURELIN	15	5-3-3-1	TANSIG-TANSIG
8	5-5-2-1	POSLIN-PURELIN	16	5-3-2-1	TANSIG-PURELIN

Table 5. Parameters of the Bat algorithm

Parameter	Value	Parameter	Value
Population size	100	Max Generations	200
Loudness	0.9	Pulse Rate	0.5
Min Frequency	0	Max Frequency	2
Alpha	0.99	Gamma	0.01

Table 6. Performance metrics for the top three ANNs combined with the Bat algorithm

Num	Topology	Train				Test			
		MAE	*RMSE*	R^2	y=ax+b	*MAE*	*RMSE*	R^2	*y=ax+b*
1	Bat-ANN 2L(5-5)	0.006	0.030	0.88	y = 0.9942x + 0.0052	0.017	0.038	0.82	y = 1.0933x – 0.0091
2	Bat-ANN 2L(3-2)	0.020	0.028	0.87	y = 0.9176x + 0.0185	0.023	0.026	0.87	y = 0.7933x + 0.0417
3	Bat-ANN 2L(4-3)	0.010	0.015	0.96	y = 0.9862x + 0.0029	0.010	0.016	0.95	y = 0.9555x + 0.0127

To illustrate the performance of the Bat-ANN 2L(4-3) model, Figure 5 displays the calculated values of the model compared to their experimental counterparts (ground truth data) for the training set, while Figure 6 presents a similar trend for the testing set. Figure 7 shows the corresponding results for all data, training and testing, for the 71 samples. In each diagram the line of perfect agreement (i.e., $y=x$) is also displayed. It can be observed that most data points are close to the line of perfect agreement, which indicates the model's ability to predict the data with reasonable accuracy.

Figure 4. The architecture of the ANN with topology 5-4-3-1

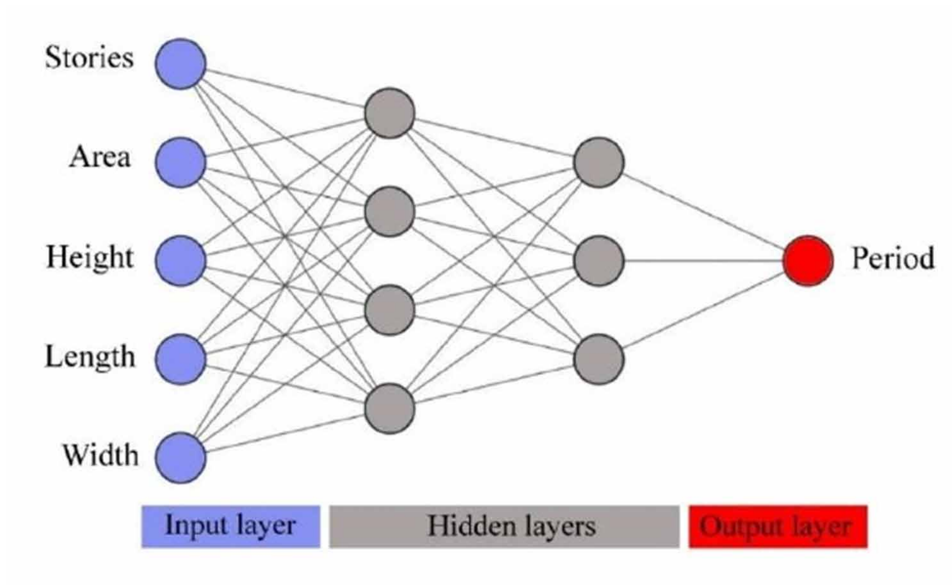

Figure 5. Experimental (ground truth) vs calculated values of the Bat-ANN 2L(4-3) model's fundamental period (training data)

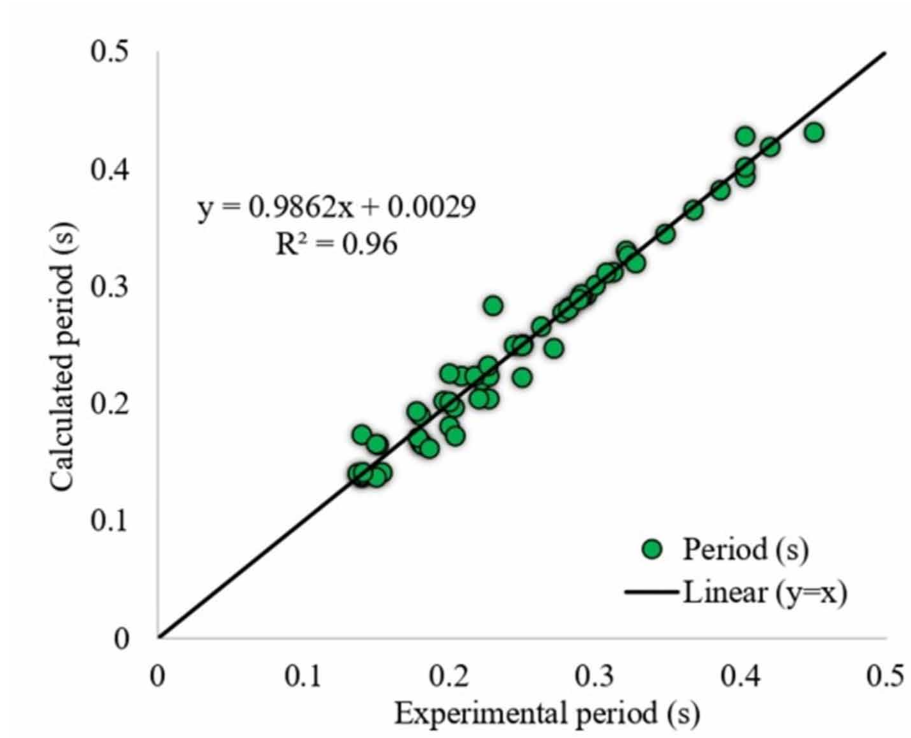

Figure 6. Experimental (ground truth) vs calculated values of the Bat-ANN 2L(4-3) model's fundamental period (testing data)

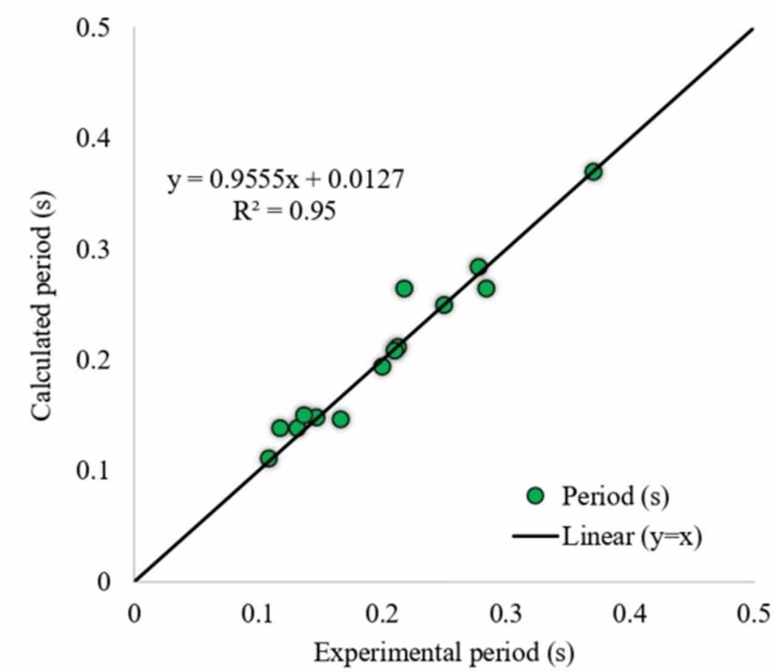

Figure 7. Experimental (ground truth) vs calculated values of the Bat-ANN 2L(4-3) model's fundamental period (all data)

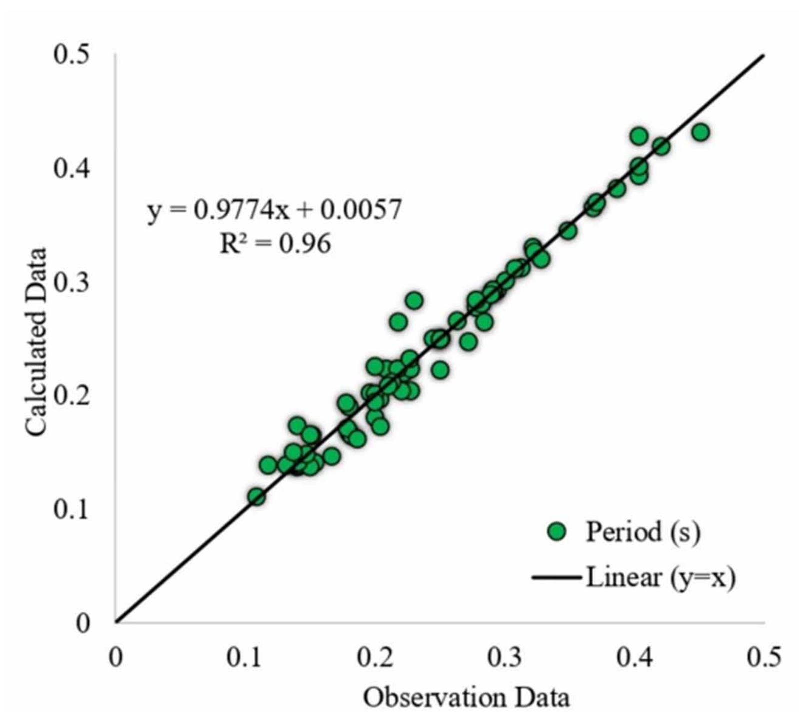

ANN Model Combined With PSO Algorithm

The PSO technique was used to train the same 16 ANN architectures specified in Table 4 in order to identify the best-performing PSO-ANN scheme. Table 7 provides the PSO algorithm parameters used in the study. The optimization parameters employed for reducing the errors in the ANNs weights of the PSO algorithm, shown in Table 7, were selected based on recommendations from a previous study (Sadowski et al., 2019). Table 8 presents the top three models and the corresponding statistical assessment measures, as well as the slope of the straight line, used for all data sets.

Table 7. The PSO algorithm parameters

Parameter	Value	Parameter	Value
Max iterations	100	Swarm size	200
Cognition Coefficient	2	Social Coefficient	2

Table 8. Performance metrics for the top three ANNs combined with the PSO algorithm

Model	All datasets			
	MAE	*RMSE*	R^2	$y = ax + b$
PSO-ANN 2L(5-5)	0.014	0.026	0.90	$y = 0.9238x + 0.0159$
PSO-ANN 2L(4-4)	0.013	0.038	0.83	$y = 1.0176x + 0.0017$
PSO-ANN 2L(5-3)	0.038	0.053	0.57	$y = 0.568x + 0.1004$

The PSO-ANN model with the best performance was the PSO-ANN 2L(5-5) model with 5 neurons in each hidden layer, exhibiting an R^2 value equal to 0.90 and indicating reasonable accuracy. The results of this model are presented in Figure 8 where the values of the experimental periods are on the horizontal axis (ground truth values) and the PSO-ANN predicted values are plotted on the vertical axis.

Nonlinear regression model and the Eureqa formula

Nonlinear regression (NLR) is a type of regression analysis in statistics in which observational data are modeled using a function of the form $y = e^{ax_1 + bx_2 + \dots}$ that is a nonlinear combination of the model parameters and is function of one or more independent variables. Successive approximations are used to fit the data. In the present work, five variables are employed as independent parameters, and the fundamental period is calculated using the DataFit software. The formula $\ln(y) = a_1 \times x_1 + a_2 \times x_2 + a_3 \times x_3 + a_4 \times x_4 + a_5 \times x_5 + a_6$ is used to evaluate several equations in this study. Eq. (20) illustrates the best case.

$$\ln y = 0.1535 \times x_1 + 0.0094 \times x_2 + 0.0001 \times x_3 - 0.023 \times x_4 + 0 \times x_5 - 1.9748 \tag{20}$$

where the dependent variable y denotes the period, x_1 is the number of stories variable, x_2 is the plan area, x_3 is the story height, and x_4 and x_5 are the variables associated with the maximum length and maximum width of the buildings, respectively. It should be highlighted here that the variable x_5 (maximum width of the building) is in fact not included in the model, since it is multiplied with zero.

Figure 8. Experimental (ground truth) vs calculated values of the fundamental period for the PSO-ANN 2L(5-5) model (all data)

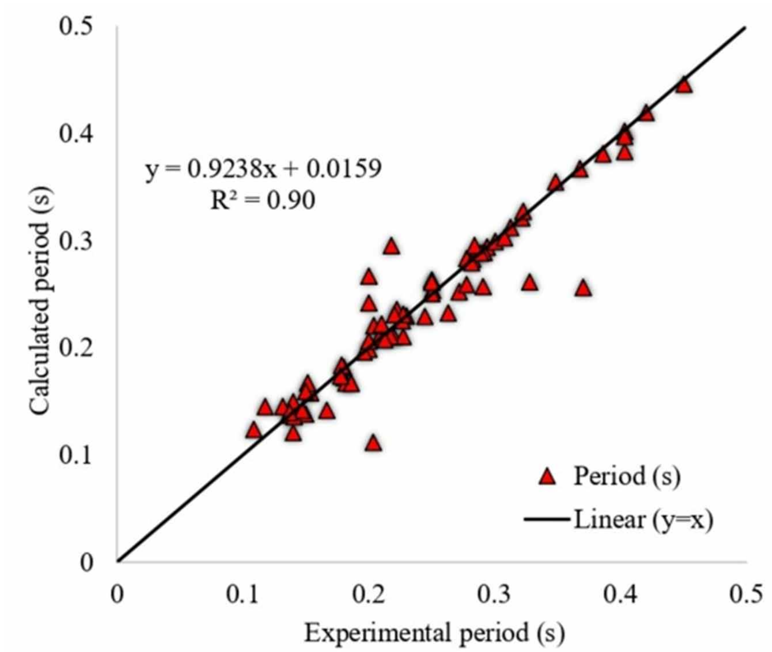

In the examined NLR model, presented in Figure 9, an R^2 value of 0.58 is obtained, and the straight-line slope is determined as 0.5869. It can be noted that a wider scatter is observed for the period in the range of 0.3 to 0.5 s, compared to the period range from 0.1 to 0.3 s.

Eureqa software (Dubčáková, 2011; Schmidt & Lipson, 2009) is a tool used to derive mathematical equations that represent varied collections of measurable inputs and outputs. A sequence of simple and sophisticated models is constructed using various mathematical operations such as addition, subtraction, multiplication, and trigonometric functions. The best-fitting data model with the least amount of error can then be chosen according to the procedures for developing mathematical models using the software. Prior to the search for suitable models, it is necessary to select the mathematical operators that will be utilized to build the models. In the beginning, basic mathematical operations such as addition and multiplication are selected to formulate the model for every parameter. If the model does not fit the data precisely, then additional operators including trigonometric and logarithmic functions may be added, and the procedure is repeated until the most precise model is finally achieved (Al-Subhi, 2020). This paper presents a mathematical equation obtained using the Eureqa software, to estimate the fundamental period as presented in Eq. (21).

$$y = 0.0704 + (0.0517 \times x_1) + \frac{0.0786 \times cos\left(0.325 \times x_3 + cos\left(x_2 + 0.135 \times x_4 - 0.344 \times x_1\right)\right)}{x_1} \quad (21)$$

Where the dependent variable y denotes the period, x_1 is the number of stories, x_2 is the area, x_3 is the height, and x_4 is the maximum length. In the mathematical model obtained from the Eureqa software (Figure 10), the R^2 value is equal to 0.65, and the slope of the straight line is 0.7114. The scatter trend found with Eureqa is somewhat similar to the one of the NLR model with slightly better correlation between the measured and the calculated period.

Figure 9. Experimental (ground truth) vs calculated values of the fundamental period for the NLR model (all data)

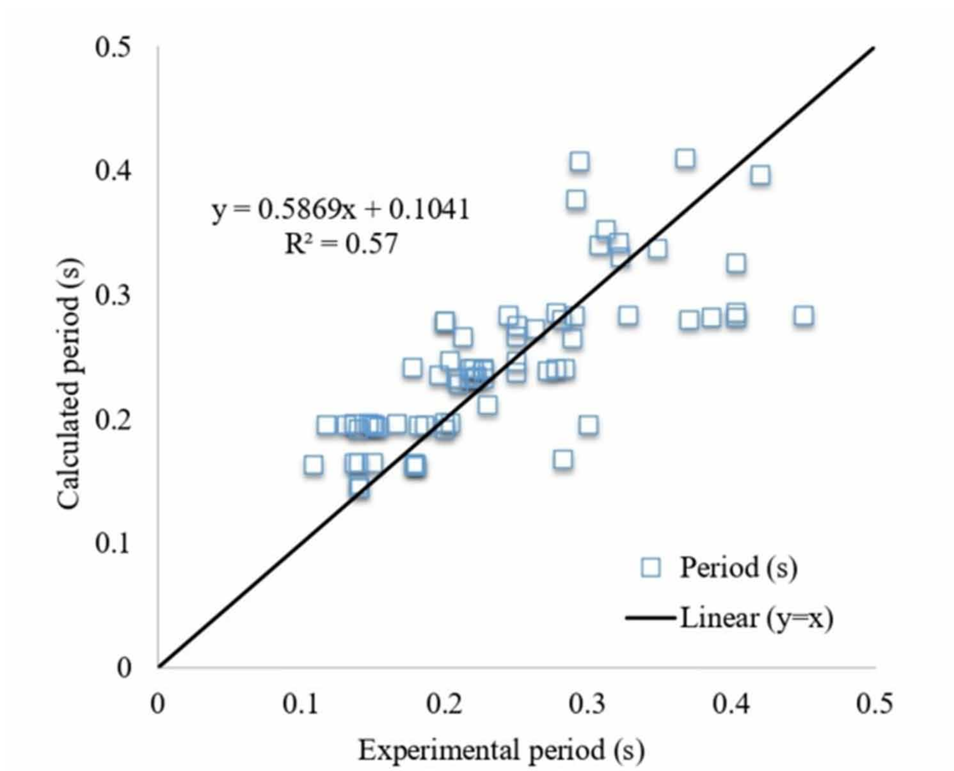

NBCC Standard Code Formula

The suitability of contemporary building code formulas to estimate the fundamental period of a structure has been discussed in the introduction section. This section provides a measure of the ability of the empirical formula in the NBCC (NRC/IRC, 2015) to predict the period of the sample buildings used in the current study. It can be observed from Figure 11 that a wide scatter is present in the data, indicating the limitation of the building code expression being a function of the building height, only.

Figure 10. Experimental (ground truth) vs calculated values of the fundamental period for the Eureqa model (all data)

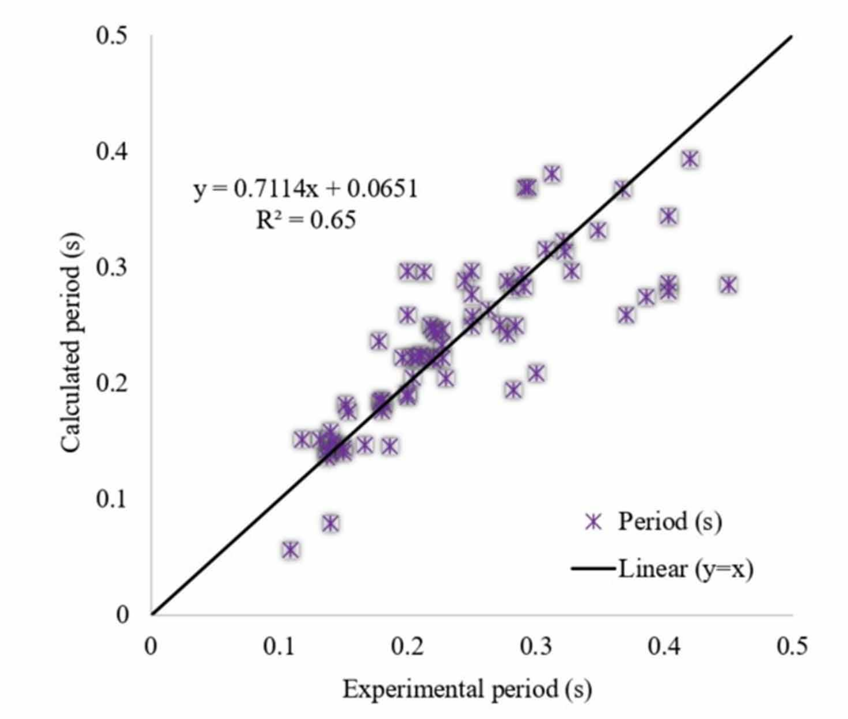

Figure 11. Experimental vs calculated values of the fundamental period for the NBCC standard (all data)

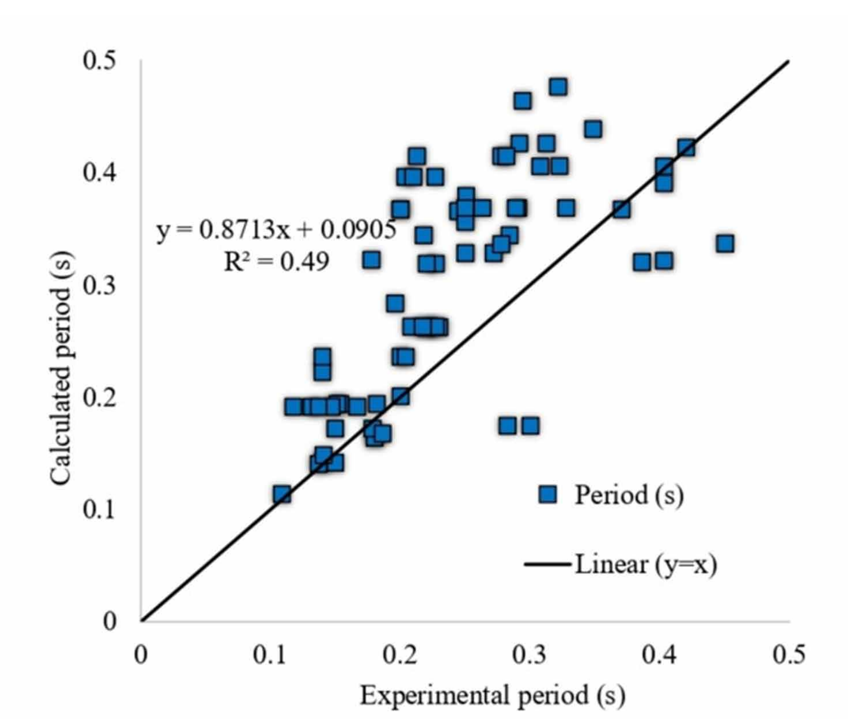

Comparison Between the Various Models

The best performing models for each category, i.e. (i) Bat-ANN, (ii) PSO-ANN, (iii) NBCC, (iv) Eureqa equation, and (v) NLR are compared based on the *MAE* and *RMSE* error metrics values, to evaluate their overall performance. The results are presented in Table 8, and they show that the Bat-ANN model provides better performance and precision for predicting the building period followed by the PSO-ANN, Eureqa equation, NLR, and then the NBCC model.

Table 8. Error metric values of the different models

No	Topology	Train set			Test set			All data		
		MAE	RMSE	R^2	MAE	RMSE	R^2	MAE	RMSE	R^2
1	NLR	0.037	0.052	0.58	0.049	0.054	0.64	0.039	0.053	0.58
2	Eureqa equation	0.030	0.047	0.66	0.042	0.053	0.53	0.032	0.049	0.65
3	NBCC	0.074	0.090	0.49	0.085	0.105	0.57	0.076	0.094	0.50
4	PSO-ANN 2L(5-5)	0.012	0.021	0.93	0.025	0.039	0.70	0.014	0.026	0.90
5	Bat-ANN 2L(4-3)	0.010	0.015	0.97	0.010	0.016	0.95	0.010	0.015	0.97

The predictions of all models in the testing phase are shown in Figure 12, where the top part of the figure compares Bat-ANN, PSO-ANN and NBCC with the ground truth (experimental) values, and the bottom part of the figure shows the comparison between Bat-ANN, Eureqa, and NLR model vs the ground truth values.

According to the results presented in Table 8 and Figure 12, it is shown that the Bat-ANN is the most accurate model, achieving predicted values of the period which are closer to the ground truth values. The Bat-ANN model exhibits the lowest *RMSE* and *MAE* metric values in the training phase, testing phase and overall data comparisons. The same conclusions are drawn also by examining the R^2 index where the Bat-ANN model performs best with an R^2 value of 0.96 for the overall dataset.

Another way to represent the results is through the Taylor diagram, which is a mathematical representation designed to graphically indicate which of several approximate models is the most realistic (Taylor, 2001). The diagram combines three statistical quantities, namely the Centered Root Mean Square Difference (*CRMSD*), the Pearson correlation coefficient R and the Standard Deviation σ in a single diagram that is easy to read and interpret (Elvidge et al., 2014). Details on the formulas used for the calculation of these three quantities can be found in the work of (Plevris et al., 2022). The Taylor diagram of the models examined in the current study is presented in Figure 13, where the ground truth results are represented with the "Reference" point. It can again be observed that the Bat-ANN model demonstrates once again the best performance, being the one closest to the reference point.

Figure 12. Comparison between the experimental results and the various models, for the test data

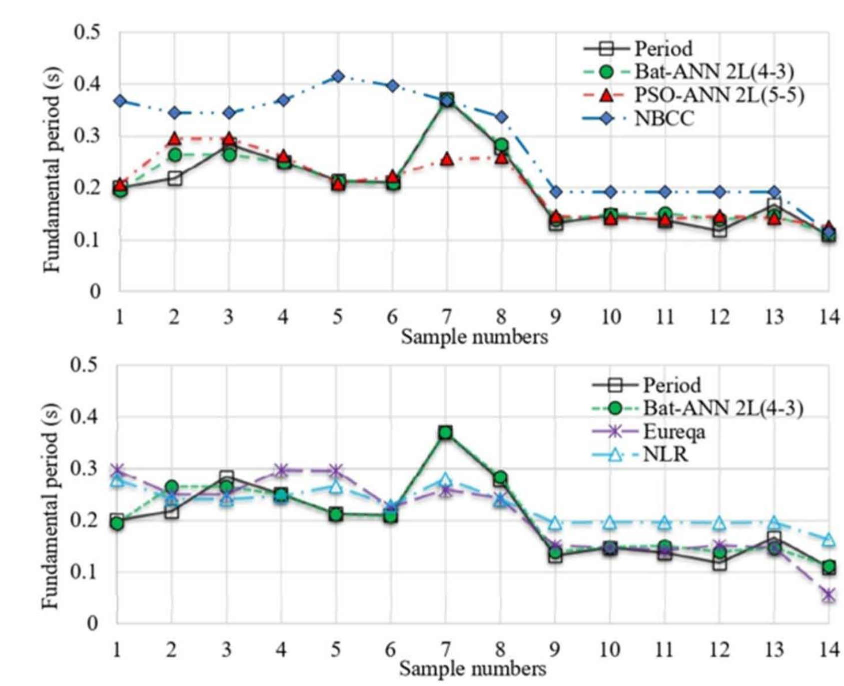

Figure 13. Taylor diagram of the examined models for the estimation of the fundamental period

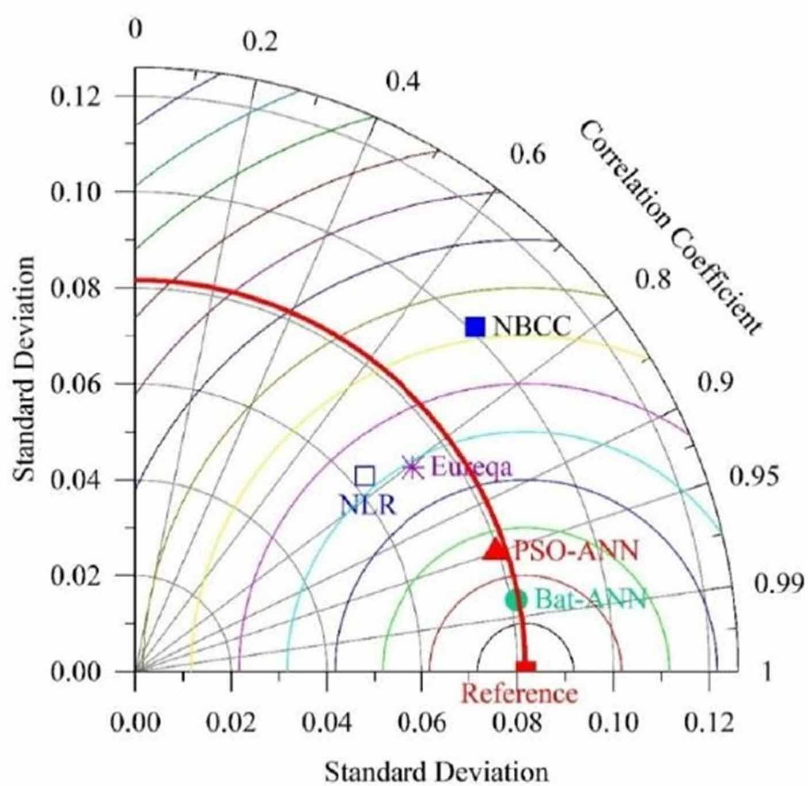

CONCLUSION

The fundamental period of a building is an important parameter required for the base shear estimation of seismic design. This paper presents an ANN model developed to predict the fundamental period of light-frame wood buildings, implementing the Bat algorithm based on reported data-set of periods obtained from 71 buildings. Sixteen Bat-ANN models, having two hidden layers, were developed. The Bat-ANN model that demonstrated the best performance was the Bat-ANN 2L network (4-3), with a 5-4-3-1 network architecture. The selection of this specific model was predicated on its performance, providing the lowest values of mean absolute error (*MAE*) and root mean squared error (*RMSE*) among all other models. This model was compared to other models, including the PSO-ANN scheme, the formula of the National Building Code of Canada (NBCC), an equation obtained from the Eureqa software, and a Non-linear regression (NLR) model. The PSO-ANN scheme was also examined with 16 variations, and the best variation was found to be that corresponding to a 5-5-5-1 network architecture. The bat algorithm showed the best fit of the data set with R^2 value of 0.96 for all data, while the corresponding R^2 value for the best PSO-ANN scheme was 0.90 for all data. The other models, including NLR, Eureqa, and NBCC, demonstrated lower accuracy and showed wider scatter than the BAT-ANN and PSO-ANN. Therefore, the proposed Bat-ANN model can be considered as a reliable, robust and accurate tool for predicting the fundamental period of wooden buildings.

ACKNOWLEDGMENT

This research received no specific grant from any funding agency in the public, commercial, or not-for-profit sectors.

REFERENCES

Aalimahmoody, N., Bedon, C., Hasanzadeh-Inanlou, N., Hasanzade-Inallu, A., & Nikoo, M. (2021). BAT Algorithm-Based ANN to Predict the Compressive Strength of Concrete—A Comparative Study. *Infrastructures*, *6*(6), 80. doi:10.3390/infrastructures6060080

Ahmad, A., Plevris, V., & Khan, Q.-u.-Z. (2020). Prediction of Properties of FRP-Confined Concrete Cylinders Based on Artificial Neural Networks. *Crystals*, *10*(9), 1-22. doi: 10.3390/cryst10090811

Ahmadi, M., Kheyroddin, A., Dalvand, A., & Kioumarsi, M. (2020). New empirical approach for determining nominal shear capacity of steel fiber reinforced concrete beams. *Construction & Building Materials*, *234*, 117293. doi:10.1016/j.conbuildmat.2019.117293

Ahmadi, M., Kheyroddin, A., & Kioumarsi, M. (2021). Prediction models for bond strength of steel reinforcement with consideration of corrosion. *Materials Today: Proceedings*, *45*, 5829–5834. doi:10.1016/j.matpr.2021.03.263

Al-Subhi, A. (2020). Parameters estimation of photovoltaic cells using simple and efficient mathematical models. *Solar Energy*, *209*, 245–257. doi:10.1016/j.solener.2020.08.079

Asteris, P. G., & Plevris, V. (2013, 2013). Neural network approximation of the masonry failure under biaxial compressive stress. *ECCOMAS Special Interest Conference - SEECCM 2013: 3rd South-East European Conference on Computational Mechanics, Proceedings*. IACM. doi:10.7712/130113.4411.S2158

Asteris, P. G., & Plevris, V. (2013, 12-14 June 2013). *Neural Network approximation of the masonry failure under biaxial compressive stress* 3rd South-East European Conference on Computational Mechanics (SEECCM III), Kos Island, Greece.

Asteris, P. G., & Plevris, V. (2017). Anisotropic masonry failure criterion using artificial neural networks. *Neural Computing & Applications*, *28*(8), 2207–2229. doi:10.1007/s00521-016-2181-3 doi:10.100700521-016-2181-3

Bardak, S., Tiryaki, S., Nemli, G., & Aydın, A. (2016). Investigation and neural network prediction of wood bonding quality based on pressing conditions. *International Journal of Adhesion and Adhesives*, *68*, 115–123. doi:10.1016/j.ijadhadh.2016.02.010

Ben Seghier, M. E. A., Corriea, J. A. F. O., Jafari-Asl, J., Malekjafarian, A., Plevris, V., & Trung, N.-T. (2021). On the modeling of the annual corrosion rate in main cables of suspension bridges using combined soft computing model and a novel nature-inspired algorithm. *Neural Computing & Applications*, *33*(23), 15969–15985. doi:10.1007/s00521-021-06199-w doi:10.100700521-021-06199-w

Bowden, G. J., Dandy, G. C., & Maier, H. R. (2005). Input determination for neural network models in water resources applications. Part 1—Background and methodology. *Journal of Hydrology (Amsterdam)*, *301*(1), 75–92. doi:10.1016/j.jhydrol.2004.06.021

Camelo, V., Beck, J. L., & Hall, J. F. (2001). *Dynamic Characteristics of Woodframe Buildings*.

Dabiri, H., Kioumarsi, M., Kheyroddin, A., Kandiri, A., & Sartipi, F. (2022). Compressive strength of concrete with recycled aggregate; a machine learning-based evaluation. *Cleaner Materials, 3*, 100044.

Dehghani, H., & Bogdanovic, D. (2018). Copper price estimation using bat algorithm. *Resources Policy*, *55*, 55–61. doi:10.1016/j.resourpol.2017.10.015

Dominguez Morales, M. (2000). *Fundamental period of vibration for reinforced concrete buildings*. University of Ottawa.

Dubčáková, R. (2011). Eureqa: Software review. *Genetic Programming and Evolvable Machines*, *12*(2), 173–178. doi:10.100710710-010-9124-z

Elvidge, S., Angling, M. J., & Nava, B. (2014). On the use of modified Taylor diagrams to compare ionospheric assimilation models. *Radio Science, 49*(9), 737-745. doi:10.1002/2014RS005435

Farsi, M. N., & Bard, P.-Y. (2004). Estimation des périodes propres de bâtiments et vulnérabilité du bâti existant dans l'agglomération de Grenoble. *Revue Française de Génie Civil*, *8*(2-3), 149–179. doi:10.1080/12795119.2004.9692601

Fathi, H., Nasir, V., & Kazemirad, S. (2020). Prediction of the mechanical properties of wood using guided wave propagation and machine learning. *Construction & Building Materials*, *262*, 120848. . doi:10.1016/j.conbuildmat.2020.120848

Gilles, D., McClure, G., & Chouinard, L. E. (2011). Uncertainty in fundamental period estimates leads to inaccurate design seismic loads. *Canadian Journal of Civil Engineering*, *38*(8), 870–880. doi:10.1139/l11-055

Gilles, D. C. (2011). *In situ dynamic characteristics of reinforced concrete shear wall buildings*. McGill University.

Goel Rakesh, K., & Chopra Anil, K. (1997). Period Formulas for Moment-Resisting Frame Buildings. *Journal of Structural Engineering*, *123*(11), 1454–1461. doi:10.1061/(ASCE)0733-9445(1997)123:11(1454)

Goel Rakesh, K., & Chopra Anil, K. (1998). Period Formulas for Concrete Shear Wall Buildings. *Journal of Structural Engineering*, *124*(4), 426–433. doi:10.1061/(ASCE)0733-9445(1998)124:4(426)

Hafeez, G., Doudak, G., & McClure, G. (2018). Establishing the fundamental period of light-frame wood buildings on the basis of ambient vibration tests. *Canadian Journal of Civil Engineering*, *45*(9), 752–765. doi:10.1139/cjce-2017-0348

Hafeez, G., Doudak, G., & McClure, G. (2019). Dynamic characteristics of light-frame wood buildings. *Canadian Journal of Civil Engineering*, *46*(1), 1–12. doi:10.1139/cjce-2017-0266

Hafeez, G., Mustafa, A., Doudak, G., & McClure, G. (2014). Predicting the Fundamental Period of Light-Frame Wood Buildings. *Journal of Performance of Constructed Facilities*, *28*(6), A4014004. doi:10.1061/(ASCE)CF.1943-5509.0000519

Kandiri, A., Sartipi, F., & Kioumarsi, M. (2021). Predicting Compressive Strength of Concrete Containing Recycled Aggregate Using Modified ANN with Different Optimization Algorithms. *Applied Sciences (Basel, Switzerland)*, *11*(2), 485. doi:10.3390/app11020485

Kennedy, J., & Eberhart, R. (1995). Particle swarm optimization *IEEE International Conference on Neural Networks*, Piscataway, NJ, USA.

Lagaros, N. D., & Papadrakakis, M. (2004). Learning improvement of neural networks used in structural optimization. *Advances in Engineering Software*, *35*(1), 9–25. doi:10.1016/S0965-9978(03)00112-1

Lagomarsino, S. (1993). Forecast models for damping and vibration periods of buildings. *Journal of Wind Engineering and Industrial Aerodynamics*, *48*(2), 221–239. doi:10.1016/0167-6105(93)90138-E

Lee, L.-H., Chang, K.-K., & Chun, Y.-S. (2000). Experimental formula for the fundamental period of RC buildings with shear-wall dominant systems. *The Structural Design of Tall Buildings, 9*(4), 295-307.

Li, J., & Heap, A. D. (2008). *A Review of Spatial Interpolation Methods for Environmental Scientists.* G. Australia.

NRC/IRC. (2015). *National Building Code of Canada 2015*. National Research Council of Canada, Institute for Research in Construction.

Panthi, B., Dahal, P., Shrestha, P., & Thapa, K. B. (2021). Fundamental period of RC buildings with infill walls in Nepal. *Asian Journal of Civil Engineering*, *22*(5), 983–993. doi:10.100742107-021-00359-y

Paz, M., & Leigh, W. (2004). Uniform Building Code 1997: Equivalent Lateral Force Method. In M. Paz & W. Leigh (Eds.), *Structural Dynamics: Theory and Computation* (pp. 699–729). Springer US. doi:10.1007/978-1-4615-0481-8_23

Pham, D. T., & Liu, X. (1995). *Neural Networks for Identification, Prediction and Control*. Springer. doi:10.1007/978-1-4471-3244-8

Plevris, V. (2009). *Innovative computational techniques for the optimum structural design considering uncertainties*. National Technical University of Athens.

Plevris, V., & Asteris, P. (2015). Anisotropic failure criterion for brittle materials using Artificial Neural Networks. 5th International Conference on Computational Methods in Structural Dynamics and Earthquake Engineering (COMPDYN 2015), Crete Island, Greece. doi:10.7712/120115.3537.3648

Plevris, V., & Asteris, P. G. (2014). Modeling of masonry compressive failure using Neural Networks OPT-i 2014. *1st International Conference on Engineering and Applied Sciences Optimization, Proceedings.* ASPETE.

Plevris, V., & Asteris, P. G. (2014). Modeling of Masonry Failure Surface under Biaxial Compressive Stress Using Neural Networks. *Construction & Building Materials*, *55*, 447–461. doi:10.1016/j.conbuildmat.2014.01.041

Plevris, V., Bakas, N. P., Markeset, G., & Bellos, J. (2017, June 15-17). Literature review of masonry structures under earthquake excitation utilizing machine learning algorithms *6th ECCOMAS Thematic Conference on Computational Methods in Structural Dynamics and Earthquake Engineering (COMPDYN 2017)*, Rhodes, Greece. 10.7712/120117.5598.18688

Plevris, V., & Papadrakakis, M. (2011). A Hybrid Particle Swarm – Gradient Algorithm for Global Structural Optimization. *Computer-Aided Civil and Infrastructure Engineering*, *26*(1), 48–68. doi: 10.1111/j.1467-8667.2010.00664.x

Plevris, V., & Solorzano, G. (2021, 28-30 June). *Prediction of The Eigenperiods of MDOF Shear Buildings using Neural Networks.* 8th ECCOMAS Thematic Conference on Computational Methods in Structural Dynamics and Earthquake Engineering (COMPDYN 2021), Athens, Greece. doi:10.7712/120121.8755.20415

Plevris, V., Solorzano, G., & Bakas, N. P. (2019, 24-26 June). *Literature review of historical masonry structures with machine learning.* 7th International Conference on Computational Methods in Structural Dynamics and Earthquake Engineering (COMPDYN 2019), Crete, Greece. doi:10.7712/120119.7018.21053

Plevris, V., Solorzano, G., Bakas, N. P., & Ben Seghier, M. E. A. (2022, 5-9 June). *Investigation of performance metrics in regression analysis and machine learning-based prediction models.* 8th European Congress on Computational Methods in Applied Sciences and Engineering (ECCOMAS 2022), Oslo, Norway. doi:10.23967/eccomas.2022.15510.23967/eccomas.2022.155

Plevris, V., & Tsiatas, G. (2018). Computational Structural Engineering: Past Achievements and Future Challenges. *Frontiers in Built Environment*, *4*(21), 1–5. doi:10.3389/fbuil.2018.00021

Sadowski, Ł., Nikoo, M., Shariq, M., Joker, E., & Czarnecki, S. (2019). The Nature-Inspired Metaheuristic Method for Predicting the Creep Strain of Green Concrete Containing Ground Granulated Blast Furnace Slag. *Materials (Basel)*, *12*(2), 293. doi:10.3390/ma12020293 PMID:30658508

Schmidt, M., & Lipson, H. (2009). Distilling Free-Form Natural Laws from Experimental Data. *Science*, *324*(5923), 81–85. doi:10.1126/science.1165893 doi:10.1126cience.1165893 PMID:19342586

Shadbahr, E., Aminnejad, B., & Lork, A. (2021). Determining post-fire residual compressive strength of reinforced concrete shear walls using the BAT algorithm. *Structures, 32*, 651-661. doi: 10.1016/j.istruc.2021.03.002

Sharib, S., Ahmad, N., Plevris, V., & Ahmad, A. (2021, 28-30 June 2021). *Prediction Models for Load Carrying Capacity of RC Wall through Neural Network*. 14th ECCOMAS Thematic Conference on Evolutionary and Deterministic Methods for Design, Optimization and Control (EUROGEN 2021), Athens, Greece. doi:10.7712/140121.7956.18529

Solorzano, G., & Plevris, V. (2021). *Design of Reinforced Concrete Isolated Footings under Axial Loading with Artificial Neural networks.* 14th ECCOMAS Thematic Conference on Evolutionary and Deterministic Methods for Design, Optimization and Control (EUROGEN 2021), Streamed from Athens, Greece. doi:10.7712/140121.7955.18448

Srivastava, S., & Sahana, S. K. (2019). Application of Bat Algorithm for Transport Network Design Problem. *Applied Computational Intelligence and Soft Computing*, *2019*, 9864090. doi:10.1155/2019/9864090

Taylor, K. E. (2001). Summarizing multiple aspects of model performance in a single diagram. *Journal of Geophysical Research*, *106*(D7), 7183–7192. doi:10.1029/2000JD900719

Tiryaki, S., & Aydın, A. (2014). An artificial neural network model for predicting compression strength of heat treated woods and comparison with a multiple linear regression model. *Construction & Building Materials*, *62*, 102–108. doi:10.1016/j.conbuildmat.2014.03.041